A multiscale model of the cardiovascular system that incorporates baroreflex control of chronotropism, cell-level contractility, and vascular tone

Running title: Multiscale modeling of baroreflex function

Hossein Sharifi [1]

Charles K. Mann [1]

Jonathan F. Wenk [1,2]

Kenneth S. Campbell [3]

[1] Department of Mechanical Engineering, University of Kentucky, Lexington, KY

[2] Department of Surgery, University of Kentucky, Lexington, KY

[3] Department of Physiology and Division of Cardiovascular Medicine, University of Kentucky, Lexington, KY

Abstract

Multiscale models of the cardiovascular system can provide new insights into physiological and pathological processes. Models that incorporate molecular-level effects may be particularly useful for clinical applications because they can predict the functional consequences of pharmaceuticals that modulate the properties of molecules and/or the rate at which they undergo reactions. PyMyoVent is a computer model that bridges from molecular to organ-level function and simulates a left ventricle pumping blood through the systemic circulation. Initial work with PyMyoVent focused on the End Systolic Pressure Volume Relationship and ranked potential therapeutic strategies by their impact on contractility. This manuscript extends PyMyoVent by adding baroreflex control of arterial pressure. The reflex algorithm is inspired by the underlying biology. It uses an afferent signal derived from arterial pressure to drive a kinetic model that mimics the net result of neural processing in the medulla and cell-level responses to autonomic drive. The kinetic model outputs control signals that are constrained between limits that represent maximum parasympathetic and maximum sympathetic drive and which modulate heart rate, intracellular Ca^{2+} dynamics, the molecular-level function of both the thick and the thin myofilaments, and vascular tone. Simulations show that the algorithm can regulate mean arterial pressure at set-points ranging from ~30 to ~150 mmHg as well as maintaining arterial pressure when challenged by rapid changes in blood volume or sudden increases in aortic resistance.

Introduction

Multiscale models of the cardiovascular system can provide new insights into physiological and pathophysiological processes (1). Numerous groups are also trying to deploy them to improve the diagnosis and treatment of disease (2, 3). Models that incorporate molecular-level mechanisms may be particularly valuable for clinical applications because they can predict the effects induced by pharmaceuticals that alter the biophysical properties of molecules and/or the rate at which they undergo reactions.

Many current models of the cardiovascular system assume that changes in cell-level contractility produce corresponding changes in circulatory pressure. Models of this type will predict that omecamtiv mecarbil, a positive myotrope that enhances myosin force generation (4, 5), will increase arterial pressure. *In vivo*, of course, the situation may be more complicated. In people, baroreceptors in the aortic arch and carotid sinuses fire action potentials at rates that indicate pressure. These signals are transmitted to the medulla which responds by modulating sympathetic and parasympathetic drive. This creates a feedback mechanism, termed the baroreflex, that continually adjusts chronotropism (heart rate), contractility, and vascular function to provide short-term regulation of arterial pressure (6).

Accordingly, if a person with a normal baroreflex is treated with a myotrope that enhances contractility, systolic pressure may not increase to the same extent as it would in an experiment using an isolated working heart. Instead, the baroreflex may down-regulate chronotropism, cell-level Ca^{2+}-handling, and vascular tone to compensate for the enhanced force-generating capacity of the myosin heads. Instead of elevating cardiac output (which is intrinsically linked to arterial pressure), the system-level responses to the myotrope might include a slower heart-rate (and thus a potential decrease in myocardial energy use) and reduced vascular tone.

This manuscript adds baroreflex control to the multiscale model previously described by Campbell et al. (7). The control algorithm is inspired by the underlying biology and is based on a kinetic model that is driven by an afferent signal derived from arterial pressure. The kinetic model mimics the net result of neural processing in the medulla and signaling pathways in effector cells, and outputs control signals that are constrained between limits which represent maximum sympathetic and maximum parasympathetic drive. In turn, the control signals modulate heart rate, intracellular Ca^{2+} dynamics, the molecular-level function of both the thick and the thin filaments, and vascular tone. As shown in the results section, the algorithm can regulate mean arterial pressure at set-points ranging from 30 to 150 mmHg, as well as maintaining arterial pressure when challenged by rapid changes in total blood volume. The model also responds to elevated aortic resistance by increasing sympathetic drive, and thus heart rate, contractility, and vascular tone.

Methods

Overview

The model described here is called PyMyoVent. As originally described by Campbell et al. (7), the framework uses a pacing stimulus to initiate a Ca^{2+} transient, that drives a myofilament-level model of contraction called MyoSim (8, 9). The contraction model predicts ventricular wall stress which is transformed into chamber pressure via Laplace's law. Finally, the chamber pumps blood through a closed circulation mimicked using a series of resistances and compliant compartments. Together, these modules scale from molecular to organ-level function.

Campbell et al.'s initial publication (7) investigated how system-level behavior (metrics such as cardiac output and systolic arterial pressure) varied as module-level parameters (including ion channel permeabilities and myosin rate constants) were varied. Heart rate was kept constant throughout these simulations. The current work extends the original framework by implementing a baroreflex (Figure 1). Specifically, heart rate and selected module level parameters were adjusted via negative feedback algorithms to drive arterial pressure towards a user-defined set-point. More details about the model for the Ca^{2+} transient and the baroreflex are provided immediately below. The other modules have already been described in detail (7).

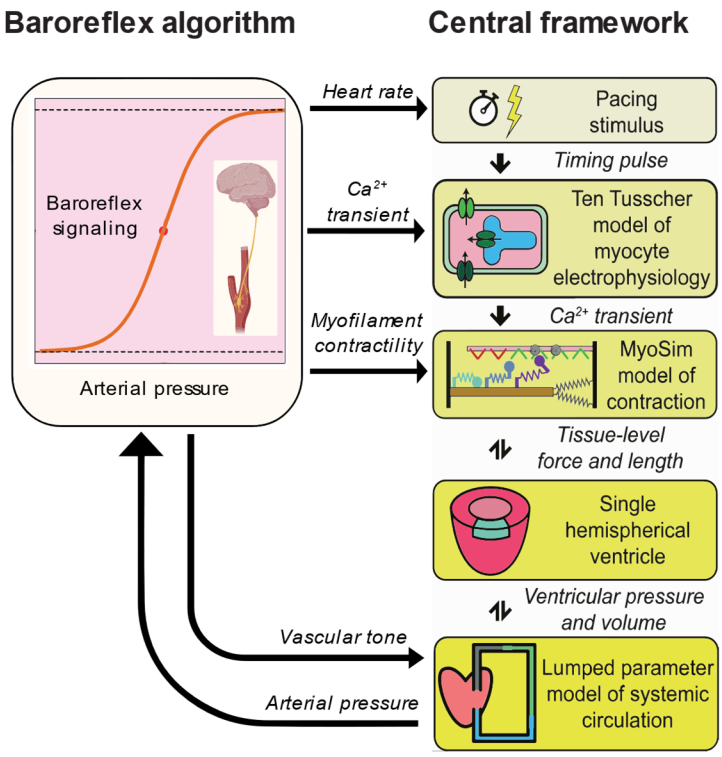

Fig 1: Overview of the PyMyoVent framework. The baroreflex algorithm monitors the arterial pressure predicted by the multiscale model and modulates heart rate, intracellular Ca^{2+} transients, myofilament contractility, and vascular tone in an attempt to drive the arterial pressure towards a user-defined setpoint. Adapted from Campbell et al. (7).

Ca^{2+} transient

The team's prior work used ten Tusscher et al.'s model of myocyte electrophysiology (10) to simulate Ca^{2+} transients. That model is based on 17 state variables and is very sophisticated. It also takes a long time to solve. Initial tests showed that these calculations slowed the overall speed of PyMyoVent simulations.

Since PyMyoVent does not utilize most of the state variables predicted by ten Tusscher et al.'s model, it was substituted for this work with a much simpler two-compartment module. Specifically, the rates of change of the Ca^{2+} concentrations in the sarcoplasmic reticulum (Ca_{SR}) and the myofilament space (Ca_{myo}) were given by:

$$\frac{dCa_{SR}(t)}{dt} = k_{SERCA}Ca_{myo}(t) - (k_{leak} + A(t)k_{act})Ca_{SR}(t) \quad (1)$$

$$\frac{dCa_{myo}(t)}{dt} = -\frac{d(Ca_{SR}(t))}{dt} \quad (2)$$

where the total Ca^{2+} concentration inside the cell $Ca_{total} = Ca_{SR} + Ca_{myo}$ was kept constant, k_{SERCA} set the rate at which Ca^{2+} is pumped into the sarcoplasmic reticulum, k_{leak} defines a continual leak of Ca^{2+} into the myofilament space, and k_{act} controls the release of Ca^{2+} when the ryanodine receptors are open. A(t) is a pulse wave that is zero except for brief periods of duration t_{open} when A(t) is equal to one. These openings are initiated by the pacing stimuli that occur at time-intervals of t_{RR} and thus determine heart-rate.

Fig S1 in Supplementary Material shows that with appropriately chosen parameters, this simple two compartment model simulates Ca^{2+} transients that are very similar to those calculated by Ten Tusscher et al.'s more sophisticated framework under steady-state conditions.

Baroreflex

Baroreflex control was implemented using an algorithm inspired by the underlying biology. Arterial pressure ($P_{arteries}$) was transduced into a normalized afferent signal (B_a) via the sigmoidal relationship

$$B_a(t) = \frac{1}{1+e^{-S(P_{arteries}(t)-P_{set})}} \quad (3)$$

where P_{set} is the setpoint for arterial pressure, and S defines the slope of the function around its midpoint. B_a thus imitates the output of the baroreceptors and varies during the cardiac cycle due to the pulsatile nature of the arterial pressure signal.

In people, the medulla uses information encoded in the afferent signal to modulate the magnitudes of sympathetic and parasympathetic drive. These efferent signals regulate cellular-level processes in multiple organs so that sustained excess sympathetic drive increases arterial pressure and excess parasympathetic drive decreases it. The current model simplified these complex mechanisms using a single balance signal B_b, seven distinct control signals ($B_{c,1}$, $B_{c,2}$ … $B_{c,7}$), and seven mapping functions (M_1, M_2 … M_7). As described in more detail below, the control signals and mapping functions modulated chronotropism, Ca^{2+} transients, myofilament function, and vascular tone.

The balance signal B_b is a normalized representation of the difference between sympathetic and parasympathetic efferent activity. Its rate of change was defined as

$$\frac{dB_b(t)}{dt} = \begin{cases} -k_{drive}(B_a(t) - 0.5)B_b(t) & B_a \geq 0.5 \\ -k_{drive}(B_a(t) - 0.5)\big(1 - B_b(t)\big) & B_a < 0.5 \end{cases} \quad (4)$$

where k_{drive} is a rate constant. These equations cause B_b to tend towards one when sympathetic drive dominates the control loop and towards zero when parasympathetic drive predominates. k_{drive} sets the speed at which the control signal responds to changes in arterial pressure and/or P_{set}.

The control signals $B_{c,i}$ capture how each of the seven reflex-sensitive parameters in the cardiovascular model respond to the balance signal. Similar to equation 4, their rates of change were defined as

$$\frac{dB_{c,i}(t)}{dt} = \begin{cases} k_{control,i}(B_b(t) - 0.5)\left(1 - B_{c,i}(t)\right) & B_b \geq 0.5 \\ k_{control,i}(B_b(t) - 0.5)B_{c,i}(t) & B_b < 0.5 \end{cases} \quad (5)$$

where i ranges from 1 to 7 and $k_{control,i}$ is the rate constant for system i. These signals are also normalized and build towards a saturating value of one when sympathetic drive exceeds parasympathetic drive ($B_b > 0.5$). If parasympathetic drive prevails, B_b is less than 0.5 and the control signals fall towards zero.

The final step in the algorithm used mapping functions M_i to link the normalized control signals $B_{c,I}$ to actual parameter values. Each mapping function took the form

$$M_i\left(B_{c,i}(t)\right) = \begin{cases} M_{base,i} + \frac{1}{2}(B_{c,i}(t) - 0.5)(M_{symp,i} - M_{base,i}) & B_{c,i} \geq 0.5 \\ M_{base,i} + \frac{1}{2}\big(B_{c,i}(t) - 0.5\big)\big(M_{para,i} - M_{base,i}\big) & B_{c,i} < 0.5 \end{cases} \quad (6)$$

where $M_{base,i}$ is the default value for parameter i, and $M_{symp,i}$ and $M_{para,i}$ are its limits during maximum sympathetic and maximum parasympathetic drive respectively.

Table 1 shows the mapping relationships. The M_{base}, M_{symp} and M_{para} values for each parameter were defined in the model file (File S1 in Supplementary Material) that was used to initialize each simulation.

	Function	Maps to	Increased arterial pressure …
Chrono-tropism	M_1	t_{RR}	Lengthens inter-beat interval and slows heart rate
Calcium-handling	M_2, M_3	k_{SERCA} and k_{act}	Reduces the amplitude and prolongs the duration of Ca^{2+} transients
Sarcomere contractility	M_4, M_5	k_1 and k_{on}	Reduces myosin cycling and sensitizes the thin filaments
Vascular tone	M_6, M_7	$R_{arteriole}$ & C_{veins}	Reduces systemic afterload and increases venous compliance

Table 1: Baroreflex implementation functions

Chronotropism

Baroreflex control of heart rate was implemented by mapping M_1 to the inter-beat interval, t_{RR}. The limits $M_{symp,1}$ and $M_{para,1}$ were set to 0.33 s and 1.5 s respectively so that heart-rate was constrained between 180 and 40 beats per minute.

Cell-level contractility

Cell-level contractility was modulated using four parameters.

M_2 and M_3 mapped to k_{act} and k_{SERCA} (equation 1) respectively. The limits for these parameters were set so that increased arterial pressure reduced the amplitude and prolonged the duration of Ca^{2+} transients.

M_4 and M_5 modulated the k_1 and k_{on} parameters in the MyoSim framework (7, 9). The k_1 parameter defines how quickly myosin heads transition from the super-relaxed (SRX) to the disordered relaxed (DRX) state (11) while k_{on} is the second-order rate constant for Ca^{2+}-activation of binding sites on actin. Their limits (File S1) were set so that increased arterial pressure enhanced contractile force by biasing myosin heads towards the DRX state but desensitized the thin filament to Ca^{2+}. These relationships mimic some of the effects produced by increased phosphorylation of myosin regulatory light chain and troponin I (12, 13).

Vascular tone

M_6 and M_7 controlled arteriolar resistance ($R_{arteriolar}$) and venous compliance (C_{veins}). File S1 shows that increased arterial pressure reduced $R_{arterioles}$ and increased C_{veins}. These effects reduce afterload and preload and complete the negative feedback loop.

Implementation and computer code

Equations 4 and 5 were discretized and added to the system of ordinary differential equations that govern the PyMyoVent framework. The inter-beat interval t_{RR} was updated once per cardiac cycle. All other feedback terms were updated each time-step.

The code was written in Python using the Numpy (14), Scipy (15), and pandas (16) libraries. Full source code, examples, and scripts that reproduce the figures included in this manuscript are available at https://campbell-muscle-lab.github.io/PyMyoVent/ and via Zenodo (17).

As described by Campbell et al. (7), no attempt was made to constrain the parameters using experimental data. Instead, parameters were set to plausible values based on prior experience and typical values for a human. For example, the total blood volume for the systemic circulation was set to 4.5 liters. Similarly, for simplicity, the seven $k_{control,i}$ parameters were set to the same value so that the $B_{c,i}$ signals are identical in this work. The model could be enhanced in future work by setting different $k_{control,i}$ values for each control. This would allow components of the reflex to respond at different speeds.

The default parameter values used to initialize all the simulations and the $M_{para,i}$ and $M_{sump,i}$ limits for each mapping function are shown in File S1. Fig S2 shows the steady-state solution with these parameters for a single cardiac cycle. That figure is comparable to Fig 3 from Campbell et al. (7) and is included here for completeness. The current work focuses on the baroreflex with most of the figures showing simulations that include at least 100 heart beats. In these figures, simulated

values that change markedly during the cardiac cycle (for example, ventricular pressure) are shown as envelopes that outline the extreme values calculated for each heart-beat.

Results

Simulations of baroreflex control of arterial pressure

Figure 2 demonstrates the baroreflex algorithm that was developed in this work. The simulation was initiated with default parameters and allowed to reach steady-state. At 50 s (the first dashed vertical line on each plot), the baroreflex was activated with a set-point P_{set} of 90 mmHg. This value was above, but close to, the steady-state arterial pressure for the default parameters. Thus, the balance signal B_b only changed by a small amount when the reflex was activated. In turn, this produced a subtle change in the value of the control signals $B_{c,i}$ and minor adjustments to heart rate, vascular tone, and the parameters controlling Ca^{2+} handling and myofilament contractility. Arterial pressure reached a new steady-state determined by the baroreflex ~10 seconds after the control algorithm was initiated.

The second dashed line in each plot at 100 s marks the time at which P_{set} was increased to 130 mmHg. This perturbation induced a much larger system-level response. Note that the balance signal B_b saturated at its maximum value and took ~30 s to recover as the reflex mechanisms worked to increase arterial pressure. The increase in P_{set} raised heart rate from 73 to ~99 beats per minute and drove proportional changes in the other controlled parameters. The changes to molecular-level function underpinned substantial cell and tissue level effects. Note, for example, that the peak systolic wall stress increased from 23 to 37 kN m^{-2}.

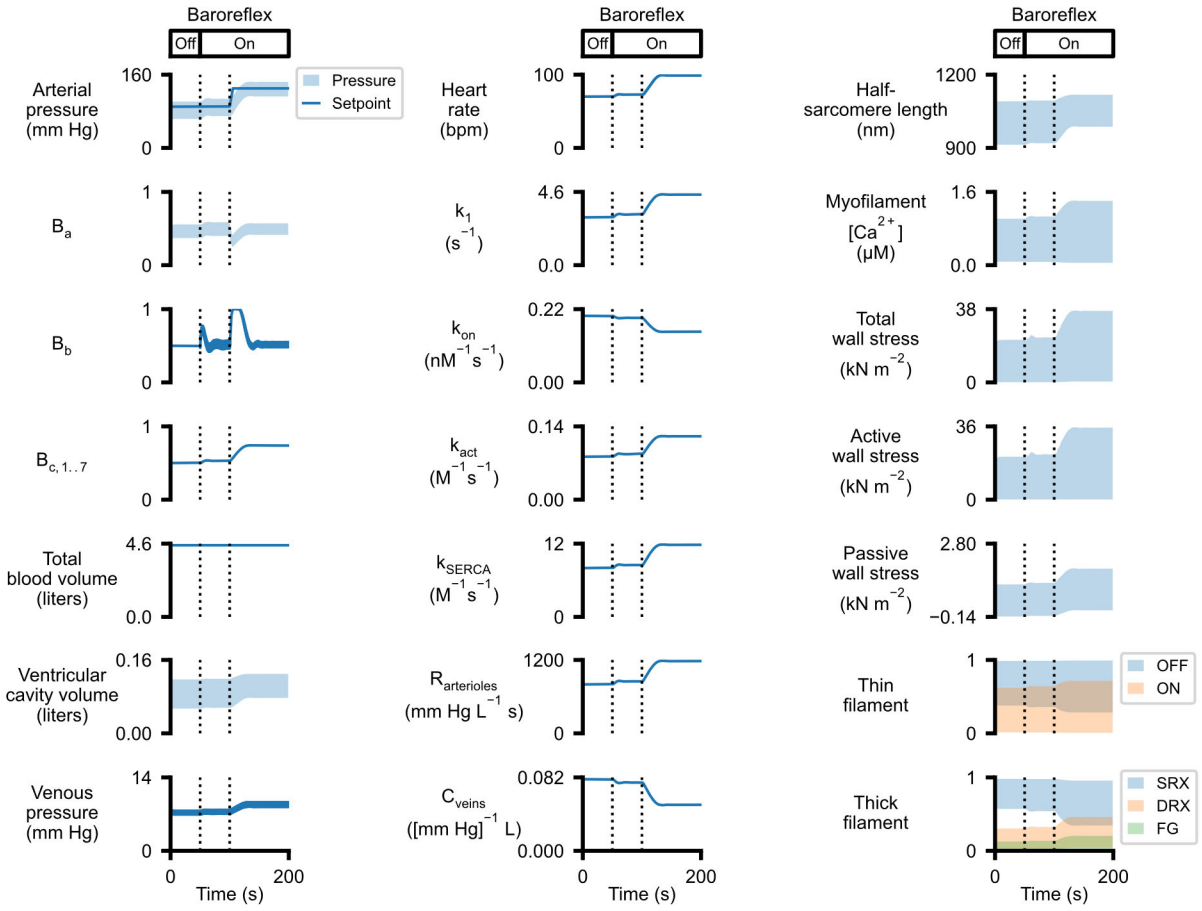

Fig 2: Baroreflex control of arterial pressure. The left hand column shows arterial pressure, the afferent (B_a), balance (B_b), and control ($B_{c,i}$) signals for the baroreflex and 3 further system-level properties. The middle column shows the 7 parameters modulated by the baroreflex. The right-hand column shows properties relevant to myocardial function. The baroreflex was initiated after 50 s (first vertical line on each plot). The baroreflex setpoint was increased from 90 to 130 mmHg after 100 s (second vertical line on each plot). The OFF and ON labels describe the status of binding sites on the thin filament. The SRX, DRX, and FG labels refer to myosin heads in the super-relaxed, disordered relaxed, and force-generating states respectively (7).

Additional simulations were run with different values of $P_{set.}$ Fig S3 in Supplementary Material shows a simulation where arterial pressure was lowered to a set-point of 50 mmHg. These calculations demonstrate that the reflex could also reduce systemic pressure by reversing the physiological effects demonstrated in Fig 2.

Further tests (not shown) demonstrated that the baroreflex could regulate arterial pressure with P_{set} values ranging from ~30 to ~150 mmHg. Fig 3 shows an example where the set-point was adjusted beyond this range to 200 mmHg. Arterial pressure increased as the reflex drove $B_{c,i}$ towards one but the controlled parameters saturated at the limits corresponding to maximum sympathetic drive before pressure reached the setpoint.

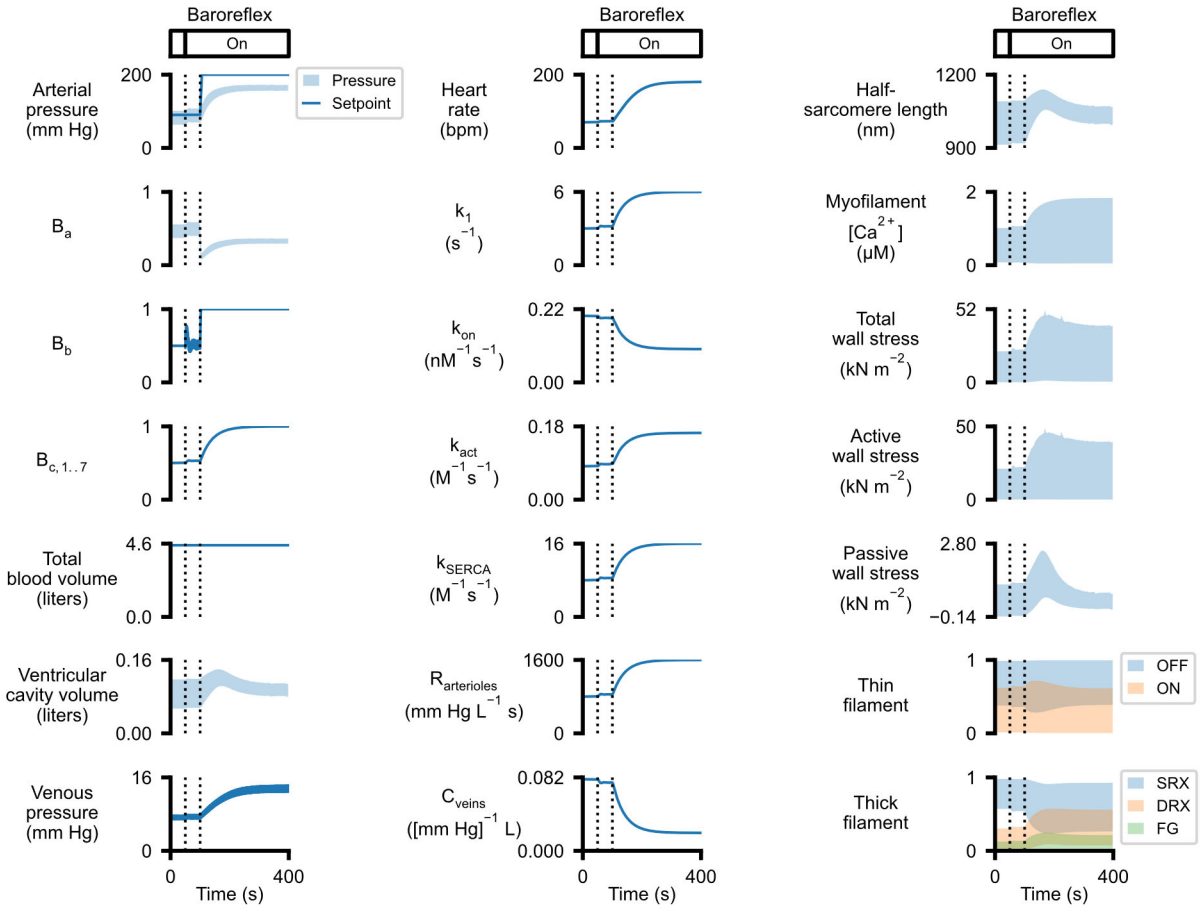

Fig 3: A simulation with P_{set} raised above the operating range. Figure panels are arranged as in Fig 2. The baroreflex was initiated after 50 s (first vertical line on each plot) with P_{set} being raised from 90 to 200 mmHg after 100s (second vertical line). This perturbation caused the balance signal B_b to increase towards 1. This drove the control signals $B_{c,i}$ towards 1 so that the reflex-controlled mechanisms saturated at levels corresponding to maximum sympathetic drive. Peak arterial pressure rose to a maximum value of 172 mmHg but the reflex -controlled responses were insufficient to raise arterial pressure to the P_{set} value of 200 mmHg.

Baroreflex control of vascular tone contributes to homeostasis

Fig 4 shows a simulation similar to the example in Fig 2 but without the vascular components of the reflex; note that the values of $R_{arterioles}$ and C_{veins} (bottom two panels in center column) remain at their defaults throughout the calculations.

When reflex control was activated (first dashed line in each panel in Fig 4), the adjustments to heart rate and contractility were sufficient to stabilize arterial pressure at the initial set-point of 90 mmHg. After 100 s (second dashed line in each panel), P_{set} was raised to 130 mmHg. This perturbation induced further increases in heart rate and contractility, and arterial pressure started to rise. However, unlike the situation in Fig 2 with the full reflex, venous compliance remained fixed so venous pressure was almost unchanged. As heart rate accelerated, the fixed venous pressure limited filling and end-diastolic volume began to fall. In turn, this compromised systolic function via Starling's law (see active wall stress in third column of Fig 4) and arterial pressure declined.

In an attempt to compensate, the baroreflex drove further increases in heart-rate and contractility but the controlled parameters reached their saturating values with $B_{c,i}$ equal to one before arterial pressure reached the set-point. Ventricular volume continued to decrease and the heart transitioned into mechanical alternans at ~220 s (shown on an expanded time-scale in Fig S4). This simulation demonstrates that vascular tone is an important component of the baroreflex.

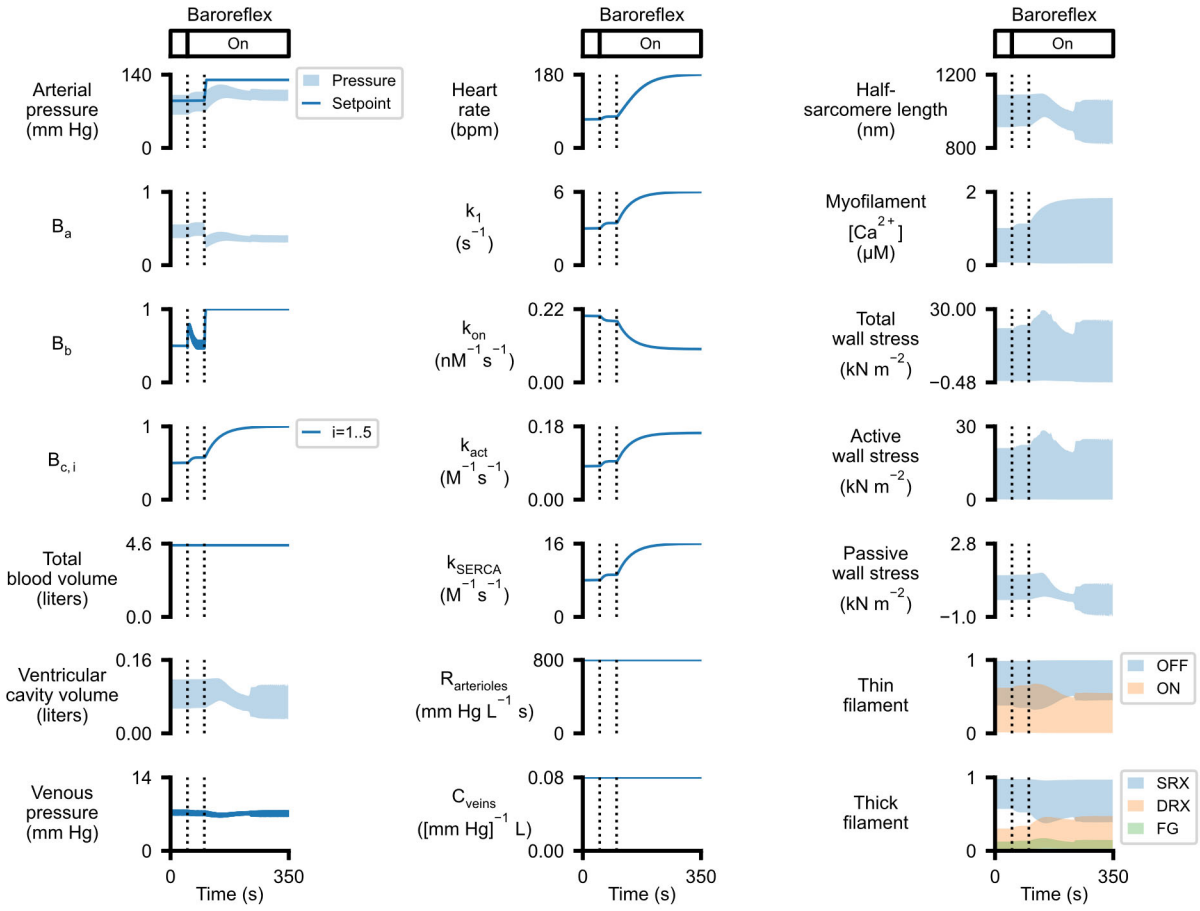

Fig 4: Simulation without baroreflex control of vascular tone. Figure panels are arranged as in Fig 2. The baroreflex was initiated after 50 s (first vertical line on each plot) with P_{set} being raised from 90 to 130 mmHg after 100s (second vertical line). This perturbation caused the reflex balance signal B_b to increase towards 1 and drove corresponding changes in heart rate, intracellular Ca^{2+}-handling, and myofilament contractility. Arteriolar resistance and venous compliance were kept constant. Consequently, venous pressure remained roughly stable and ventricular filling (shown by cavity volume (left-hand column) and half-sarcomere length (right-hand column)) became impaired as heart rate increased. The heart developed mechanical alternans ((shown on an expanded time-scale in Fig S4) at ~220 s.

The baroreflex stabilizes arterial pressure after rapid blood loss

Fig 5 shows a simulation in which 13% of the total blood volume was removed from the venous compartment while the baroreflex was active with P_{set} equal to 90 mmHg. Venous pressure dropped from 7 to 2 mmHg but the baroreflex modulated heart rate, Ca^{2+}-transients, myofilament contractility, and vascular tone to maintain arterial pressure. This simulation mimics some of the physiological responses induced by hemorrhage and demonstrates that the reflex algorithm can stabilize arterial pressure after sudden changes in total blood volume.

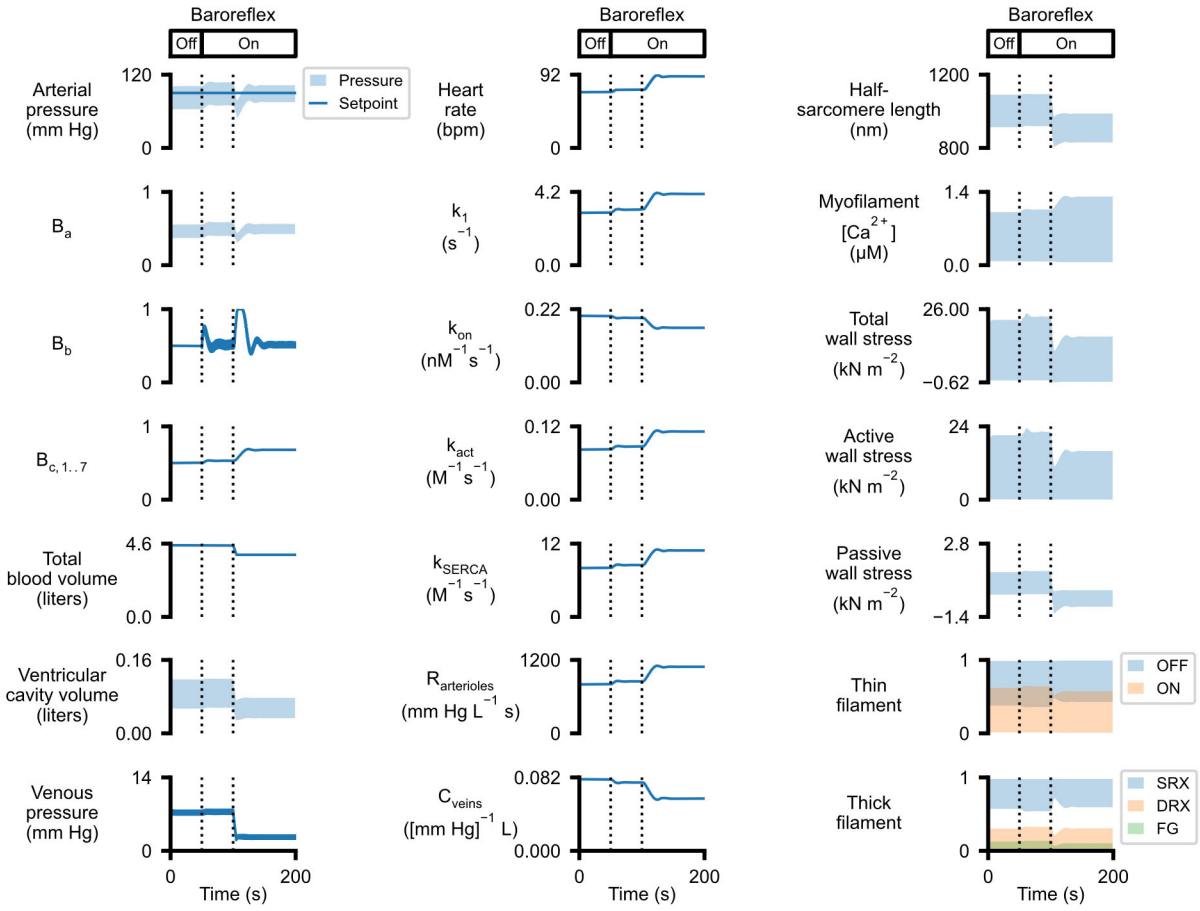

Fig 5: Simulated response to rapid blood loss. Figure panels are arranged as in Fig 2. The baroreflex was initiated after 50 s (first vertical line on each plot) with P_{set} equal to 90 mmHg. 600 ml of blood (~13% of total volume) was removed from the venous circulation between 100s (second vertical line) and 105 s. This perturbation induced rapid changes in heart rate, Ca^{2+}-handling, myofilament contractility, and vascular tone which, in concert, maintained arterial pressure at the reflex setpoint. If the baroreflex had not been active, the blood loss would have reduced arterial pressure to 66/39 mmHg (see Fig S5).

The baroreflex stabilizes arterial pressure when aortic resistance is increased

Fig 6 shows the system's response to a sudden increase in aortic resistance. This perturbation increased the pressure gradient between the ventricle and the aorta and thus mimics a sudden (and thus clinically unlikely) onset of aortic valve stenosis. The control algorithm maintained arterial pressure at the expense of a marked increase in myocardial wall stress.

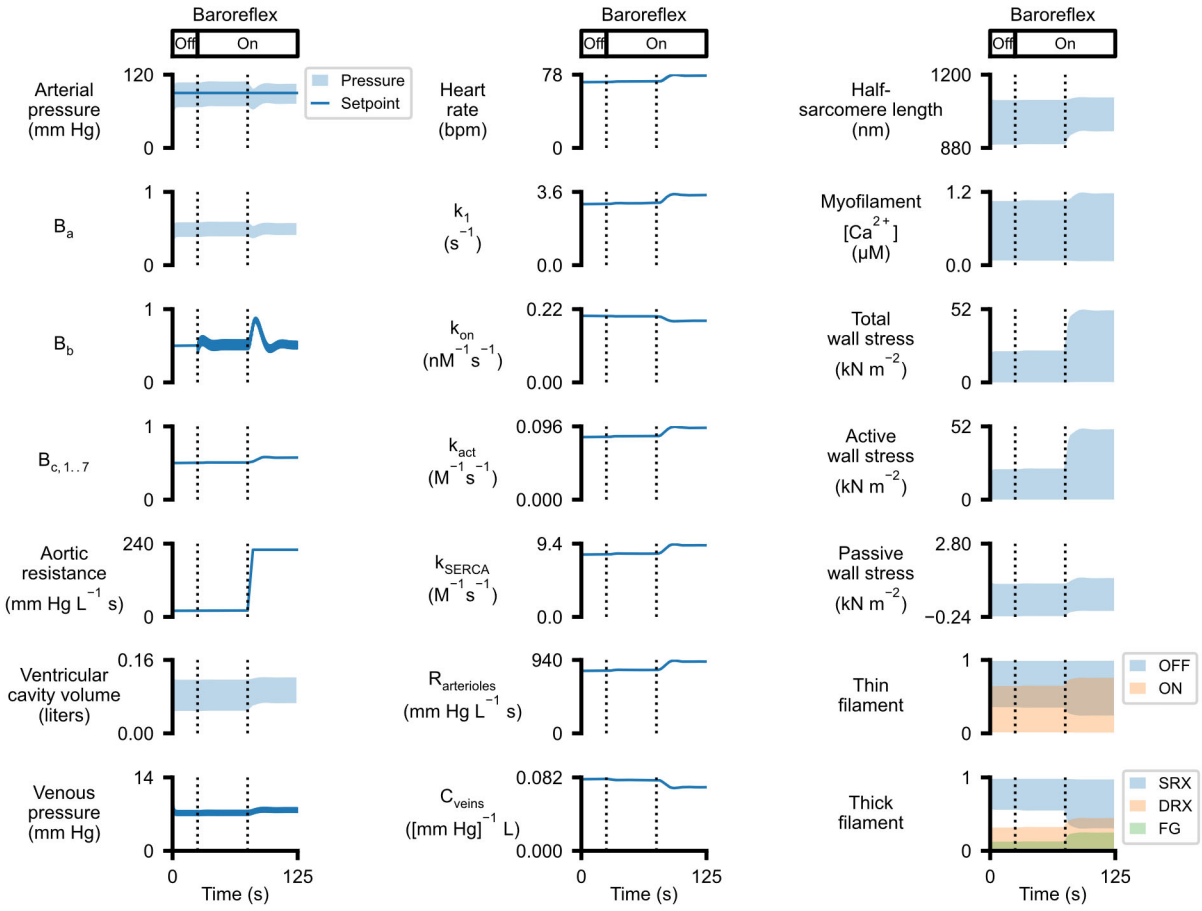

Fig 6: Simulated response to a rapid increase in aortic resistance. Figure panels are arranged as in Fig 2 except that aortic resistance is shown in place of total blood volume in the left-hand column. The baroreflex was initiated after 50 s (first vertical line on each plot) with P_{set} equal to 90 mmHg. The aortic resistance was increased from 20 to 220 mmHg L^{-1} s between 75 and 80 s. This perturbation induced changes in heart rate, Ca^{2+}-handling, myofilament contractility, and vascular tone which together maintained arterial pressure at the reflex setpoint. Peak wall stress approximately doubled following the increase in aortic resistance. Fig S6 shows the system's response to the same increase in aortic resistance without baroreflex control.

Fig 7 compares the control pressure-volume loops to those measured after the increase in aortic resistance with and without baroreflex control. This figure demonstrates that an increase in aortic resistance elevates ventricular pressure irrespective of baroreflex control. This is because the myocardium shortens more slowly when it is working against the higher resistance and is thus operating on a different portion of its force-velocity curve.

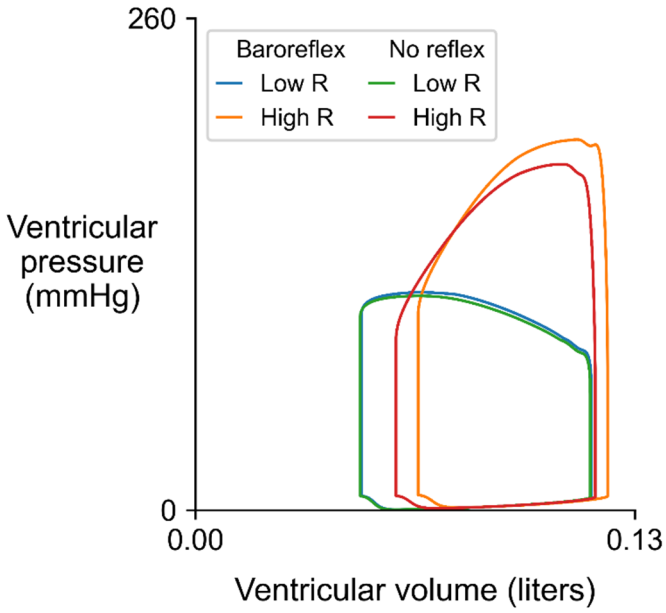

Fig 7: Simulated pressure volume loops for a ventricle pumping against control and elevated aortic resistance with and without baroreflex control. The loops show simulated data from Figs 6 and S6 with ventricular pressure plotted against ventricular volume before and after the increase in aortic resistance (R). Note that ventricular pressure increases markedly even in the absence of baroreflex control as the myocardium ejects blood against the higher resistance. The reflex accentuates this response with the increased heart rate (not visible in this plot) helping to pump more blood into the aorta. Note that the decrease in vascular compliance induced by the reflex elevates filling pressure and contributes to an increased end diastolic volume.

Discussion

This manuscript describes a mathematical model of the cardiovascular system that implements baroreflex control of arterial pressure by modulating heart rate, intracellular Ca^{2+}-handling, myofilament biophysics, and vascular tone. The control algorithm was inspired by the underlying biology and incorporates several of the molecular-level mechanisms that are known to be regulated by the autonomic nervous system. Calculations showed that the framework could maintain arterial pressure at set-points ranging from 30 to 150 mmHg and at a physiological value of 90 mmHg when challenged by sudden changes in total blood volume or a substantial increase in aortic resistance.

The simulations also demonstrated the importance of dynamic control of vascular tone. The baroreflex's ability to regulate arterial pressure was compromised when it could not adjust venous compliance in concert with heart-rate and cell-level contractility.

Comparison with prior models incorporating baroreflex control

Many other mathematical models that incorporate baroreflex control have been published. Due to the complexity of the cardiovascular system, different groups have chosen to emphasize selected mechanisms and simplified other aspects of their model. A recent paper by Rondanina and Bovendeerd (18), for example, focused on cardiac growth and implemented baroreflex control by adjusting only peripheral resistance and circulatory unstressed volume. Dupuis et al. (19) used a similar approach but chose to adjust total blood volume rather than unstressed volume in their CircAdapt-based simulations (20) of cardiac resynchronization therapy.

Other groups have added cardiac-based parameters to their baroreflex mechanisms. Jezek et al. (21) investigated system-level responses to exercise and changes in posture, and adjusted heart rate, contractility, and vascular tone in their model. Ursino implemented similar mechanisms in their pioneering work (22). Both of these papers idealized ventricle contraction using a time-varying elastance approach in which the relationship between ventricular pressure and volume varies with time during the cardiac cycle (23).

The current model uses a different strategy that takes advantage of the molecular-level mechanisms underpinning the contractile module. Specifically, in addition to modulating heart rate and vascular tone, the baroreflex control algorithm adjusts four parameters that define the magnitude and time-course of intracellular Ca^{2+} transients and the function of the thick and thin myofilaments. To the authors' knowledge, this is the first cardiovascular model in which the baroreflex algorithm directly controls molecular-level contractility rather than phenomenological relationships. This might make it easier to test how pharmaceuticals and/or genetic modifications to calcium-handling proteins and/or sarcomeric proteins affect the baroreflex.

The kinetic model described by equations 3 to 5 is also interesting because it captures several aspects of the underlying physiology in a mathematical framework. These factors include the concept of excess autonomic drive which is represented in the model by the balance signal B_b. If arterial pressure is below the reflex setpoint, the medulla increases sympathetic efferent activity and decreases parasympthatic activity. In the calculations, this is mimicked by B_b rising towards its upper limit of one. Similarly, arterial pressures greater than the reflex setpoint will increase parasympathetic activity and diminish sympathetic drive. The model mimics this behavior by driving B_b towards zero. The ordinary differential equation (equation 4) dictates how the B_b signal

evolves over time with the rate constant k_{drive} controlling how quickly the signal responds to changes in arterial pressure and setpoint.

The $B_{c,i}$ signals (equation 5) provide an additional level of control and are intended to mimic the response of the cell-level effectors to changing autonomic drive. $B_{c,5}$, for instance, modulates the second order rate constant k_{on} for Ca^{2+} activation of binding sites on the thin filament (9). In vivo, this is regulated, at least in part, by Protein Kinase A-based phosphorylation of troponin I (12). Excess sympathetic drive enhances kinase activity and, if sustained, gradually increases the proportion of troponin I molecules that are phosphorylated. The value of k_{on} when all of the troponins are phosphorylated is the $M_{symp,5}$ limit. Similarly, excess parasympathetic drive (B_b < 0.5) deactivates the kinase allowing the proportion of troponin I molecules to fall over time. The $M_{para,5}$ limit defines the k_{on} value when none of the troponin molecules are phosphorylated. The other control signals mimic similar mechanisms. In all cases, the differential equations (equation 5) allow the status of the mechanisms to evolve over time with the speed of the responses being set by the $k_{control,i}$ parameters.

Importance of vascular tone

Prototype versions of the current model attempted to regulate arterial pressure solely via chronotropism and adjustments to cell-level contractility. As demonstrated in Figs 4 and S4, these attempts were only partly successful and failed to regulate arterial pressure over a realistic physiological range.

The problem with the prototypes was that venous return did not increase with cardiac output. When the reflex was activated, contractility and heart-rate increased to elevate cardiac output and raise arterial pressure. While this strategy was successful for the first few beats, it also redistributed blood towards the arteries. Since the veins remained compliant, the pressure difference pushing blood back towards the heart dropped slightly and venous return could not sustain the increased cardiac output. End-diastolic volume started to fall with consequent reductions in stroke volume. Heart rate continued to increase in an attempt to compensate but this further compromised filling and the ventricle eventually transitioned to mechanical alternans with small and big stroke volumes on success cycles (Fig S4).

Adding reflex control of vascular tone solved this problem and allowed the algorithm to maintain arterial pressure over a wider operating range. The key addition was allowing venous compliance to drop during increased sympathetic drive. This raised venous pressure and enhanced venous return so that it could sustain long-term increases in cardiac output.

Limitations of the current model

Some of the limitations of the PyMyoVent framework have already been discussed (7). These include: the single ventricle architecture, the assumption that the ventricle is hemispherical, and the one-way coupling of the electrophysiological and contractile modules.

The baroreflex developed in this work is also greatly simplified. One of the most obvious issues is that real hearts receive dual input from both parasympathetic and sympathetic nerves while PyMyoVent uses a single B_b balance signal which reflects the efferents' difference. One of the limitations of this approach is that it prevents adjusting single reflex effectors independently of the others.

Another weakness is that the current model only incorporates a few of the mechanisms that are subject to autonomic control. The important effects of myosin binding protein-C, for instance, are ignored (24). In principle, it might be possible to replace the current MyoSim-based contractile system with a different module, such as FiberSim (25) that provides better molecular-level contractile fidelity. In practice, the added complexity might slow the calculations to an undesirable level.

Summary

PyMyoVent is a multiscale model of the cardiovascular system that can regulate arterial pressure using a baroreflex algorithm that is inspired by the underlying biology and regulates molecular-level mechanisms. The software runs on a standard laptop and is fully open-source. Interested parties are encouraged to download the software and use it in their own work. The current authors hope to use the new system to improve quantitative understanding of cardiovascular function and potentially to help accelerate the development of better therapies for patients who have cardiovascular disease.

Acknowledgements

Supported by NIH HL133359 to KSC and JFW, NIH 148785 and TR0001998 to KSC, and AHA TP135689 to KSC.

Author contributions

HS drafted the manuscript, wrote prototype versions of the code, helped develop the website and GitHub repository, and ran prototype simulations. KJM helped write prototype versions of the code. JFW helped develop the model framework and edited the manuscript. KSC planned the overall project, developed the baroreflex algorithm, wrote the final version of the code, ran the final simulations, created the figures, and finalized the manuscript.

References

1. **Niederer SA, Campbell KS, and Campbell SG**. A short history of the development of mathematical models of cardiac mechanics. *J Mol Cell Cardiol* 127: 11-19, 2019.
2. **Niederer SA, Lumens J, and Trayanova NA**. Computational models in cardiology. *Nat Rev Cardiol* 16: 100-111, 2019.
3. **Campbell KS, Yengo CM, Lee LC, Kotter J, Sorrell VL, Guglin M, and Wenk JF**. Closing the therapeutic loop. *Archives of biochemistry and biophysics* 663: 129-131, 2019.
4. **Teerlink JR, Clarke CP, Saikali KG, Lee JH, Chen MM, Escandon RD, Elliott L, Bee R, Habibzadeh MR, Goldman JH, Schiller NB, Malik FI, and Wolff AA**. Dose-dependent augmentation of cardiac systolic function with the selective cardiac myosin activator, omecamtiv mecarbil: a first-in-man study. *Lancet* 378: 667-675, 2011.
5. **Swenson AM, Tang W, Blair CA, Fetrow CM, Unrath WC, Previs MJ, Campbell KS, and Yengo CM**. Omecamtiv Mecarbil Enhances the Duty Ratio of Human beta-Cardiac Myosin Resulting in Increased Calcium Sensitivity and Slowed Force Development in Cardiac Muscle. *J Biol Chem* 292: 3768-3778, 2017.
6. **Ursino M, and Magosso E**. Short-term autonomic control of cardiovascular function: a mini-review with the help of mathematical models. *J Integr Neurosci* 2: 219-247, 2003.
7. **Campbell KS, Chrisman BS, and Campbell SG**. Multiscale Modeling of Cardiovascular Function Predicts That the End-Systolic Pressure Volume Relationship Can Be Targeted via Multiple Therapeutic Strategies. *Frontiers in physiology* 11: 1043, 2020.
8. **Campbell KS**. Dynamic coupling of regulated binding sites and cycling myosin heads in striated muscle. *J Gen Physiol* 143: 387-399, 2014.
9. **Campbell KS, Janssen PML, and Campbell SG**. Force-Dependent Recruitment from the Myosin Off State Contributes to Length-Dependent Activation. *Biophys J* 115: 543-553, 2018.
10. **ten Tusscher KH, Noble D, Noble PJ, and Panfilov AV**. A model for human ventricular tissue. *Am J Physiol Heart Circ Physiol* 286: H1573-1589, 2004.
11. **Schmid M, and Toepfer CN**. Cardiac myosin super relaxation (SRX): a perspective on fundamental biology, human disease and therapeutics. *Biol Open* 10: 2021.
12. **Solaro RJ, Henze M, and Kobayashi T**. Integration of troponin I phosphorylation with cardiac regulatory networks. *Circ Res* 112: 355-366, 2013.
13. **Kampourakis T, Sun YB, and Irving M**. Myosin light chain phosphorylation enhances contraction of heart muscle via structural changes in both thick and thin filaments. *Proc Natl Acad Sci U S A* 113: E3039-3047, 2016.
14. **van der Walt S, Colbert SC, and Varoquaux G**. The NumPy Array: A structure for efficient numerical computation. *Computing in Science and Engineering* 13: 22-30, 2011.
15. **Virtanen P, Gommers R, Oliphant TE, Haberland M, Reddy T, Cournapeau D, Burovski E, Peterson P, Weckesser W, Bright J, van der Walt SJ, Brett M, Wilson J, Millman KJ, Mayorov N, Nelson ARJ, Jones E, Kern R, Larson E, Carey CJ, Polat I, Feng Y, Moore EW, VanderPlas J, Laxalde D, Perktold J, Cimrman R, Henriksen I, Quintero EA, Harris CR, Archibald AM, Ribeiro AH, Pedregosa F, van Mulbregt P, and SciPy C**. SciPy 1.0: fundamental algorithms for scientific computing in Python. *Nat Methods* 17: 261-272, 2020.
16. **Reback J, Mendel JB, McKinney W, Bossche JVd, Augspurger T, Cloud P, Hawkins S, Young GF, Srinhrks MR, Klein A, Petersen T, Tratner J, She C, Ayd W, Hoefler P, Naveh S, Garcia M, Schendel J, Hayden A, Saxton D, Shadrach R, Gorelli ME, Li F, Jancauskas V, attack68, McMaster A, Battiston P, Seabold S, and Dong K**. pandas-dev/pandas: Pandas 1.3.2 https://doi.org/10.5281/zenodo.5203279.
17. **Campbell KS**. PyMyoVent. 2021.

18. **Rondanina E, and Bovendeerd PHM**. Stimulus-effect relations for left ventricular growth obtained with a simple multi-scale model: the influence of hemodynamic feedback. *Biomech Model Mechanobiol* 19: 2111-2126, 2020.
19. **Dupuis LJ, Arts T, Prinzen FW, Delhaas T, and Lumens J**. Linking cross-bridge cycling kinetics to response to cardiac resynchronization therapy: a multiscale modelling study. *Europace* 20: iii87-iii93, 2018.
20. **Palau-Caballero G, Walmsley J, Gorcsan J, 3rd, Lumens J, and Delhaas T**. Abnormal Ventricular and Aortic Wall Properties Can Cause Inconsistencies in Grading Aortic Regurgitation Severity: A Computer Simulation Study. *Journal of the American Society of Echocardiography : official publication of the American Society of Echocardiography* 29: 1122-1130 e1124, 2016.
21. **Jezek F, Randall EB, Carlson BE, and Beard DA**. Systems analysis of the mechanisms governing the cardiovascular response to changes in posture and in peripheral demand during exercise. *J Mol Cell Cardiol* 2021.
22. **Ursino M**. Interaction between carotid baroregulation and the pulsating heart: a mathematical model. *Am J Physiol* 275: H1733-1747, 1998.
23. **Suga H, and Sagawa K**. Instantaneous pressure-volume relationships and their ratio in the excised, supported canine left ventricle. *Circ Res* 35: 117-126, 1974.
24. **Heling L, Geeves MA, and Kad NM**. MyBP-C: one protein to govern them all. *J Muscle Res Cell Motil* 41: 91-101, 2020.
25. **Kosta S, Colli D, Ye Q, and Campbell KS**. FiberSim: a flexible open-source model of myofilament-level contraction. *bioRxiv* 2021.2006.2011.448126, 2021.